SMECTITE-TO-ILLITE ALTERATION IN SALT-BEARING BENTONITES (THE EAST SLOVAK BASIN)

M. Honty[1],*, P. Uhlík[1], V. Šucha[1], M. Čaplovičová[1], J. Franců[2], N. Clauer[3] and A. Biroň[4]

[1] Comenius University, Mlynská Dolina, 84215 Bratislava, Slovakia,
[2] Czech Geological Survey, Leitnerova 22, 658 69 Brno, Czech Republic
[3] Centre de Géochimie de la Surface (CNRS-ULP), Ecole et Observatoire des Sciences de la Terre, 67084-Strasbourg, France
[4] Institute of Geology, Severná 5, 974 01 Banská Bystrica, Slovakia

Abstract—The effect of a saline environment on illitization in volcanoclastic rocks is examined in deep boreholes in the East Slovak Basin. Based on X-ray diffraction analysis, it is concluded that illite-smectite (I-S) expandability is always less in the salt-bearing bentonites (SBB) than in the salt-free bentonites (SFB) for a given depth interval. These two lithologies can be distinguished easily by water-leachate chemistry. Within the depth interval 2100−2500 m, the expandability in SBB varies within the range 25−10% expandable with R1 and R3 ordering in SBB and 68−35% expandable with R0 ordering in SFB. In two shallow SBB samples the expandability is close to that of SFB, suggesting that salinity alone does not enhance the illitization; but salinity may enhance it when combined with higher burial temperature. Vitrinite reflectance and T_{max} of RockEval pyrolysis measured in adjacent shales confirm that the increased illitization in SBB is not due to heating and/or erosion. The model of burial and thermal history calibrated by organic maturity suggests that the same thermal history produces two different expandabilities in the two lithologies (SBB and SFB). Particle thickness measurements and K-Ar data were used to deduce the crystal growth mechanism of illitization in SBB. Whereas surface-controlled growth is typical for SFB, simultaneous nucleation and growth played a more important role in the case of SBB. The effect of a salty environment on the illitization is not yet fully understood and may have severe consequences for the utilization of bentonites as engineering barriers in radioactive waste disposal sites if salt formations used as host rocks are taken into account.

Key Words—Bentonites, Crystal-size Distribution, Diagenesis, East Slovak Basin, Illitization, Salty Environment.

INTRODUCTION

Many studies have shown that illitization of smectite is one of the best indicators for evaluation of the diagenetic degree of sedimentary rocks (*e.g.* Hower *et al.*, 1976; Środoń and Eberl, 1984; Pollastro, 1993; Środoń, 1995). Sometimes, however, non-diagenetic geological events, such as contact metamorphism (Nadeau and Reynolds, 1981) and volcanic activity (Honty *et al.*, 2002), may significantly affect the degree of illitization. In such cases, it is not possible to use illitization for tracing diagenetic events. Moreover, the nature of smectite interlayer cations, K concentration, starting material (Eberl and Hower, 1976; Whitney and Northrop, 1988; Huang *et al.*, 1993; Mosser-Ruck *et al.*, 1999), rock/water ratio (Whitney, 1990; Mosser-Ruck *et al.*, 1999) and high pH (Eberl *et al.*,1993; Bauer and Velde, 1999) may also affect the process and rate of illitization.

Some studies focus on the formation of I-S from smectite at surface conditions, in the sediments of saline lakes (Singer and Stoffers, 1980; Deconinck *et al.*, 1988; Hay *et al.*, 1991; Turner and Fishman, 1991). Turner and

Fishman (1991) found I-S having a range of expandabilities in altered tuff beds in a Jurassic lake in the Morrison Formation (Eastern Colorado Plateau, USA). The observed clays did not experience deep burial, and did not undergo hydrothermal alteration. The illite content in I-S generally increased from the margin (100−70% S) to the centre of the lake (30−0% S) following a lateral hydrochemical gradient, characterized by increasing salinity and alkalinity. The authors concluded that solution chemistry was a principal factor controlling the smectite to illite reaction at Earth's surface temperature. Illite-smectite can form from smectite at low temperatures by several ways, *e.g.* through wetting and drying (WD) cycles (Eberl *et al.*, 1986), common in the evaporitic environment of saline lakes. In the presence of K^+ ions, WD leads to irreversible fixation of K and formation of illite layers. Eberl *et al.* (1986) observed that WD in KOH solutions led to a higher proportion of collapsed layers than WD cycles of K-saturated samples in distilled water. Illite-smectite formation at elevated pH did not even require WD cycles. The formation of I-S from smectites at low temperatures and high pH was examined by Eberl *et al.* (1993), Heller-Kallai and Eberl (1997) and Bauer and Velde (1999). Heating smectites at 60°C in 0.1−1 M KOH promoted illite formation (Eberl *et al.*, 1993). The same experiment with 3 M KOH initially led to a drastic

* E-mail address of corresponding author:
honty@fns.uniba.sk

reduction in expanded layers finally leaving an amorphous product. The illite formation was more efficient in KOH compared to NaOH solutions. The decrease of smectite XRD peak intensity through experiment indicated that the smectite dissolution preceded the illite formation. The same effect was noticed by Bauer and Velde (1999). Raising the temperature from 35°C to 80°C increased the degree of illite formation, producing >40% I and ~90% illite, respectively. In general, the reaction rate increased with increasing pH, temperature and time in these studies. Eberl *et al.* (1993) pointed out that the high alkalinities of saturated KOH solutions used in their experiments are geologically unrealistic. The experiments performed under milder conditions (1 M $KHCO_3$ and 1 M K_2CO_3) at 60°C accompanied by WD showed that after six WD cycles the expandability dropped dramatically from 94 to 57% S in $KHCO_3$ and

to 50% S in K_2CO_3. However, the effect of mild alkaline solutions at higher temperatures was not studied.

The present study has been carried out with these studies in mind, but looking instead at the illitization of buried bentonites which might have been altered by saline, alkaline fluids. Saline, alkaline solutions originate in lakes of arid regions. In the case of the buried sediments, they may act as brines circulating along the faults and through pore spaces.

GEOLOGICAL SETTING

The East Slovak Basin (ESB) is a volcano-sedimentary basin located on the junction of the Western and Eastern Carpathians in the northwestern part of the Trans-Carpathian depression (Figure 1). The tectonic regime of the basin was controlled by the collision of the
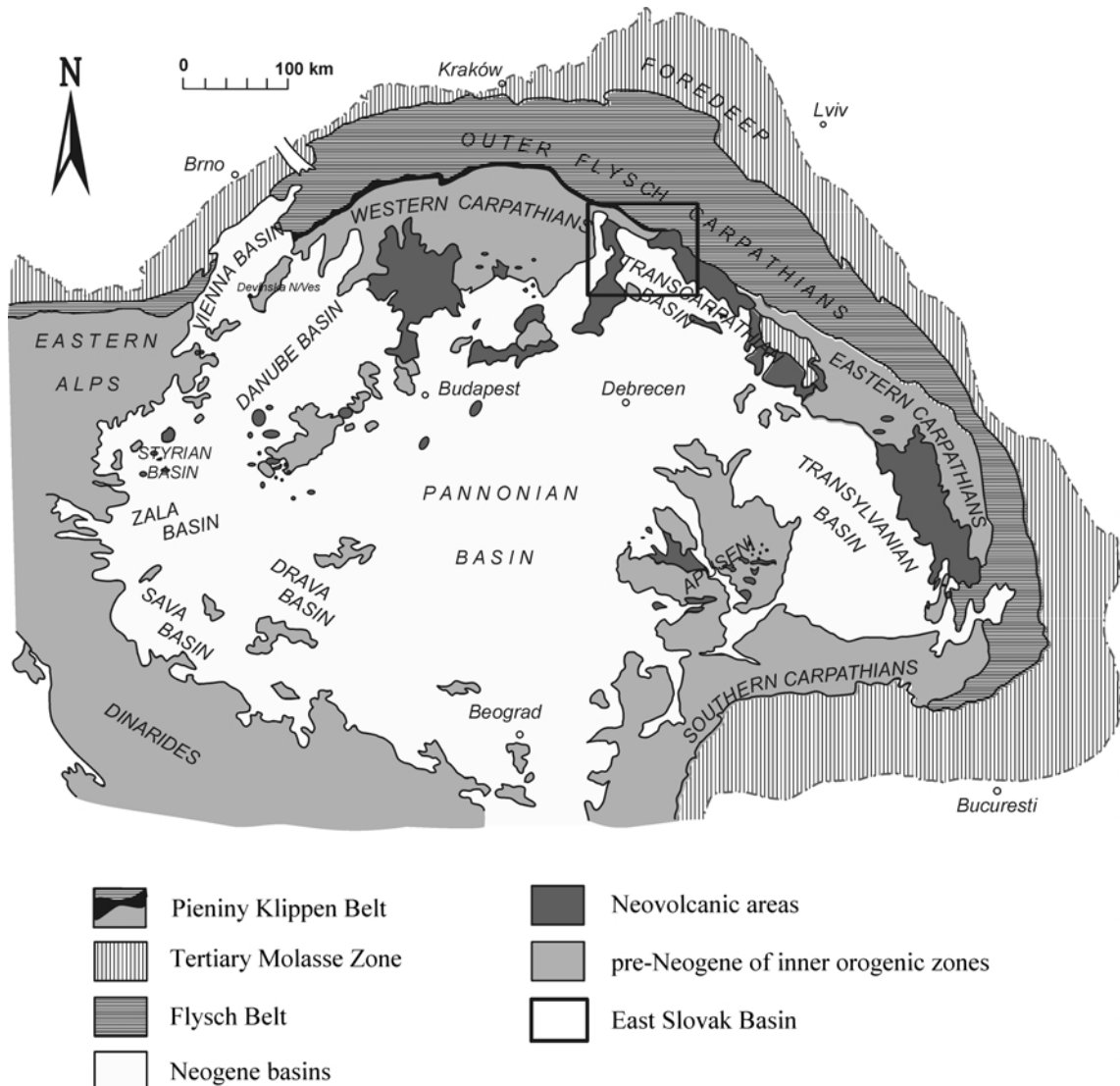

Figure 1. The position of the East Slovak Basin in the Pannonian system of Neogene basins (modified after Kováč *et al.*, 1995).

Carpathian orogen with the North European platform. The formation of strike-slip faults during Carpathian times opened the central part of the basin with pull-apart mechanism (Kováč et al., 1995). The initial stage of the crustal stretching was associated with dacitic to rhyolitic volcanic activity. Carpathian/Lower Badenian evaporites were deposited as a result of the shallowing of the marginal zone or precipitation at the water-air interface in the central part of the basin (Karoli, 1993). During the Lower Badenian, the evaporite formation shifted to the northeastern part of the basin. The lagoonal salt deposition was characterized by the rapid bottom growth of chevron and cloudy halite crystals (Karoli, 1993). During the Middle Badenian, two formations were deposited in the East Slovak Basin − the Vranov Formation and the Zbudza Formation. The Vranov Formation consists of dark gray calcareous siltstones and claystones with sporadic layers of fine-grained sands and sandstones, dark calcareous clays and tuffite layers (Rudinec, 1989; Vass and Čverčko, 1985). The formation attains a maximum thickness of 500−600 m. This sedimentary cycle terminates with relatively extensive shallow-water lagoonal salt deposition, mainly in the northern, northwestern and central parts of the ESB. The thickness of this salt-bearing sequence (the Zbudza Formation) varies between 50 and 300 m. The formation consists of saline clays, claystones, fine-grained sandstones and evaporites (halite, gypsum, anhydrite). The Upper Badenian to Lower Sarmatian synrift phase (15−12.7 Ma) is a consequence of an active subduction in the Eastern Carpathian region associated with a rollback effect of the subducted slab and as a consequence of hinterland mantle uplift accompanied by the huge volcanism of the calc-alkaline type (Lexa et al., 1993). During this time the ESB became a back-arc basin in which shallowing-upward sediments with tuff and tuffite intercalations were deposited. The final stage of the ESB rifting took place during the Upper Sarmatian (~12 Ma), followed by the culmination of volcanic activity. The sedimentary environment shows a gradual decrease of salinity, reaching brackish to lacustrine character. During Pannonian time (11.5−7.1 Ma) the sedimentation was controlled by thermal subsidence and the basin became a peripheral part of the Pannonian Basin system. The schematic lithological profile of the basin, regional names of sedimentary units, depositional environments and prevailing tectonic regime through time are shown in Figure 2.

Based on the backstripping modeling of 20 selected wells, three main periods of rapid tectonic subsidence were recognized. Rapid subsidence occurred during Carpathian, Middle Badenian and Lower Sarmathian times, separated by periods of slower subsidence. Pannonian to Quaternary history (11.5 Ma–present) shows very slow tectonic subsidence. The present-day position of the basin is well above sea level, and subsidence analyses show a late-stage uplift (Baráth et al., 1997).

For this study the most important features of the ESB are: (1) an extremely high thermal flow ($Q = 82−113$ mWm^{-2}) inducing temperatures of ~209ºC at a depth of 4 km (Král' et al., 1985); (2) the presence of intense acid to intermediate volcanism of the alkali-calcic type from the Badenian to Early Pannonian age (Vass et al., 1988); and (3) the occurrence of evaporitic (especially halite-bearing) formations during the Carpathian and Badenian times (Galamay and Karoli, 1997; Karoli et al., 1997). The map in Figure 3 shows the geographical positions of the boreholes studied, lines AA′ and BB′ represent longitudinal and transverse geological profiles across the basin, presented in Figure 4. The borehole numbers correspond to those listed in Table 1.

MATERIALS AND METHODS

All samples used for this study were taken from different boreholes at a depth interval from 31 to 3602 m (Table 1). All are of Miocene age (23.4−5.3 Ma). Basically, two types of samples were examined: salt-bearing and salt-free bentonites. The term bentonite is being used in this study for fine-grained to coarse-grained, altered rhyolitic to andesitic tuffs. Light microscopy revealed the features typical of volcanic rocks: corroded quartz, biotite, zonal feldspars and volcanic glass. Four claystones (shales) accompanying the SBB were used for the study of organic matter. The expandability values of the SFB and shales used in this study were adopted from the paper of Šucha et al. (1993). The main criterion to distinguish bentonites from shales is the presence of detrital dioctahedral mica in the latter. Samples containing detrital mica (according to XRD data) were not considered to be altered volcanoclastic rocks. Macroscopically detectable salinity, subsequently verified by chemical analysis, was used to distinguish between SBB and SFB.

The bulk samples were crushed to pass a 0.16 mm sieve, then soaked in distilled water and disintegrated in an ultrasonic bath. The samples were treated with a sodium acetate buffer, hydrogen peroxide and sodium dithionite (Jackson, 1975). The <2 μm fraction was separated by sedimentation and the <0.2 μm fraction by centrifugation. Finer fractions were separated for selected samples using a continuous-flow high-speed centrifuge Beckman J2-MC. Excess soluble salts were removed by centrifugation followed by dialysis. The XRD analysis of oriented <2 μm fractions (air dried and ethylene glycolated) and random specimens of bulk rock were carried out using a Philips 1075 diffractometer with a Ni filter and CuKα radiation. The expandability (% S$_{XRD}$) was determined according to the methods described by Środoń (1981) and Dudek and Środoń (1996).

The chemical compositions of 12 leachates of SBB and SFB were determined. 2 g of <0.16 mm bulk sample were mixed with 100 mL of distilled water and shaken
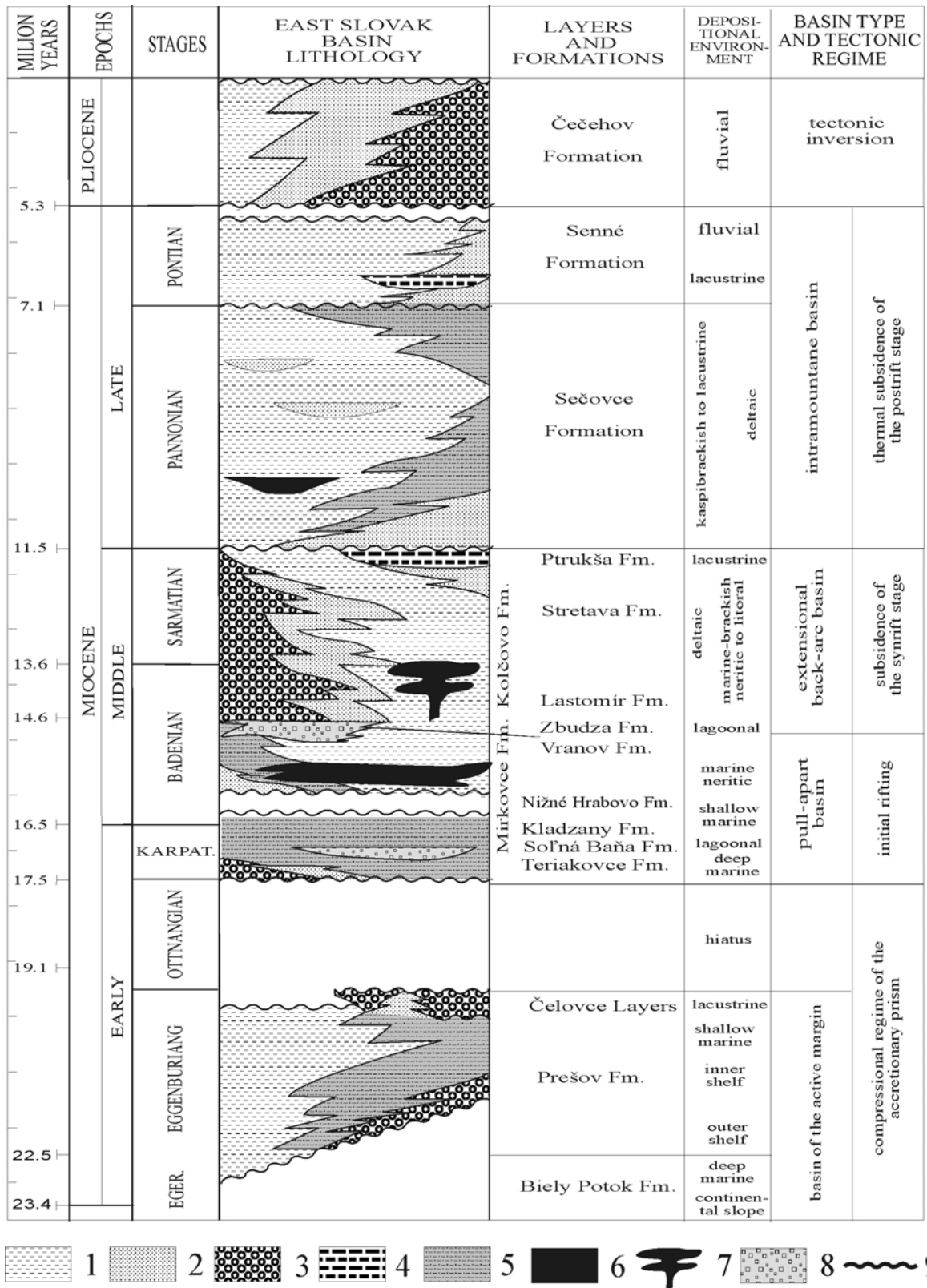
Figure 2. The schematic lithological profile of the East Slovak Basin. Legend: (1) pelites, (2) sandstones, (3) conglomerates, (4) lignite/coal, (5) silts, (6) rhyolite tuffs, (7) rhyolites, (8) evaporites, (9) hiatus/erosion (modified after Vass and Čverčko, 1985).
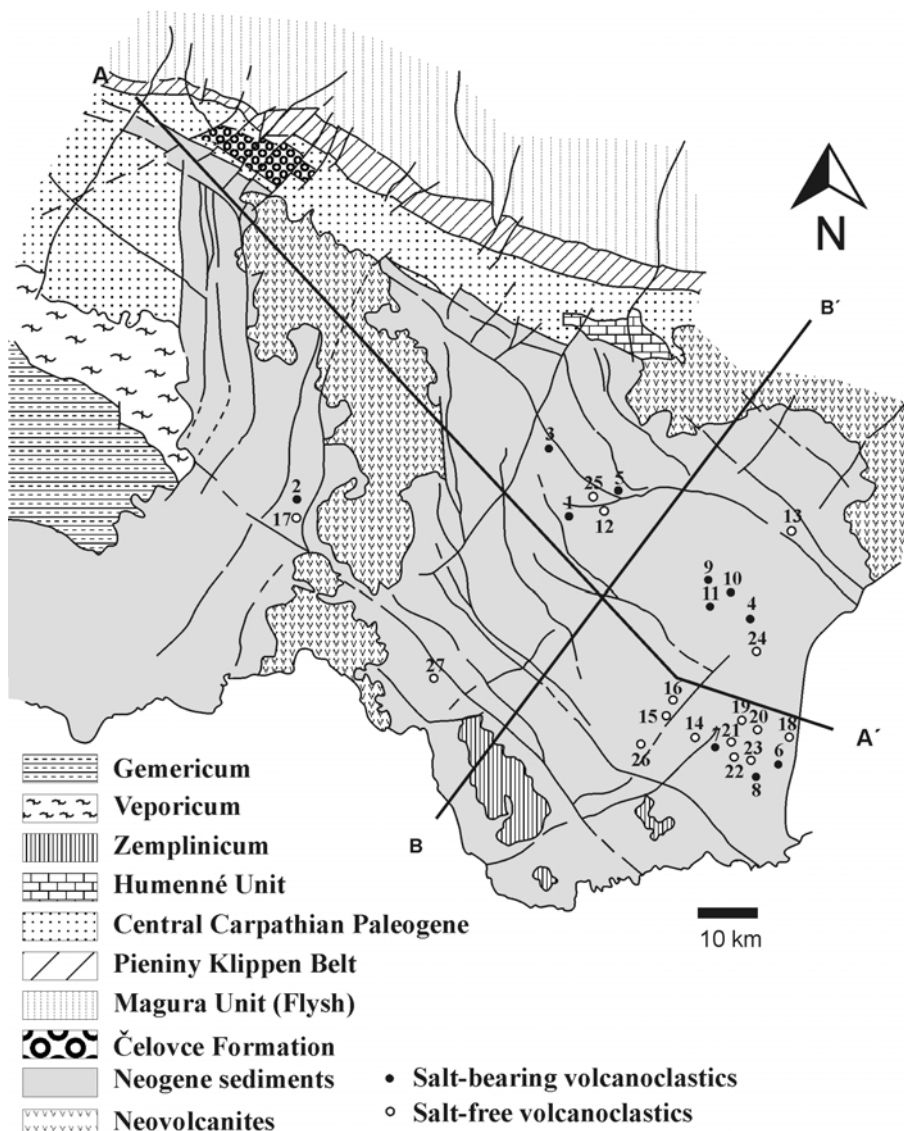
Figure 3. Map showing the location of the boreholes studied. AA′ – longitudinal and BB′ – transverse cross sections presented in Figure 4. For borehole numbers see Table 1.

for 24 h. After treatment, the sample and solution were separated by high-speed centrifugation. Calcium, Mg, K and Na were analyzed in an acetylene-air flame by atomic absorption spectroscopy using a Perkin Elmer 1100 atomic absorption spectrometer with an uncertainty of ±1%. Chlorides were analyzed by titration, and SO$_4$ gravimetrically, with analytical uncertainties of ±5% and ±0.5%, respectively.

The scanning electron microscopy (SEM) images of bulk-rock thin-sections were acquired using a JEOL JXA-733 microscope. The images were taken at a magnification of 100−720 ×.

The illite fundamental particle thicknesses and their distributions were determined for the <2 µm fraction by XRD of PVP-10 intercalated clays (Eberl et al., 1998a) and high-resolution transmission electron microscopy

(HRTEM) of clays intercalated with the same polymer (Uhlík et al., 2000). Samples were analyzed using a Siemens D500 XRD system with a graphite monochromator, CuKα radiation, a range of 2−10º2θ, a step size of 0.02º2θ, and a count time of 5 s per step. The resulting first-order reflections were measured by the Bertaut-Warren-Averbach (BWA) method (Drits et al., 1998) using the computer program MudMaster (Eberl et al., 1996). This method gives accurate measurements of mean thicknesses for I-S clays that are <50% expandable, because XRD is not able to detect monolayers (Eberl et al., 1998a). The HRTEM-PVP technique, which detects monolayers, requires intercalation of clays by PVP-10 as a pretreatment before embedding in resin for HRTEM. A more detailed description of the sample preparation can be found in Uhlík et al. (2000).
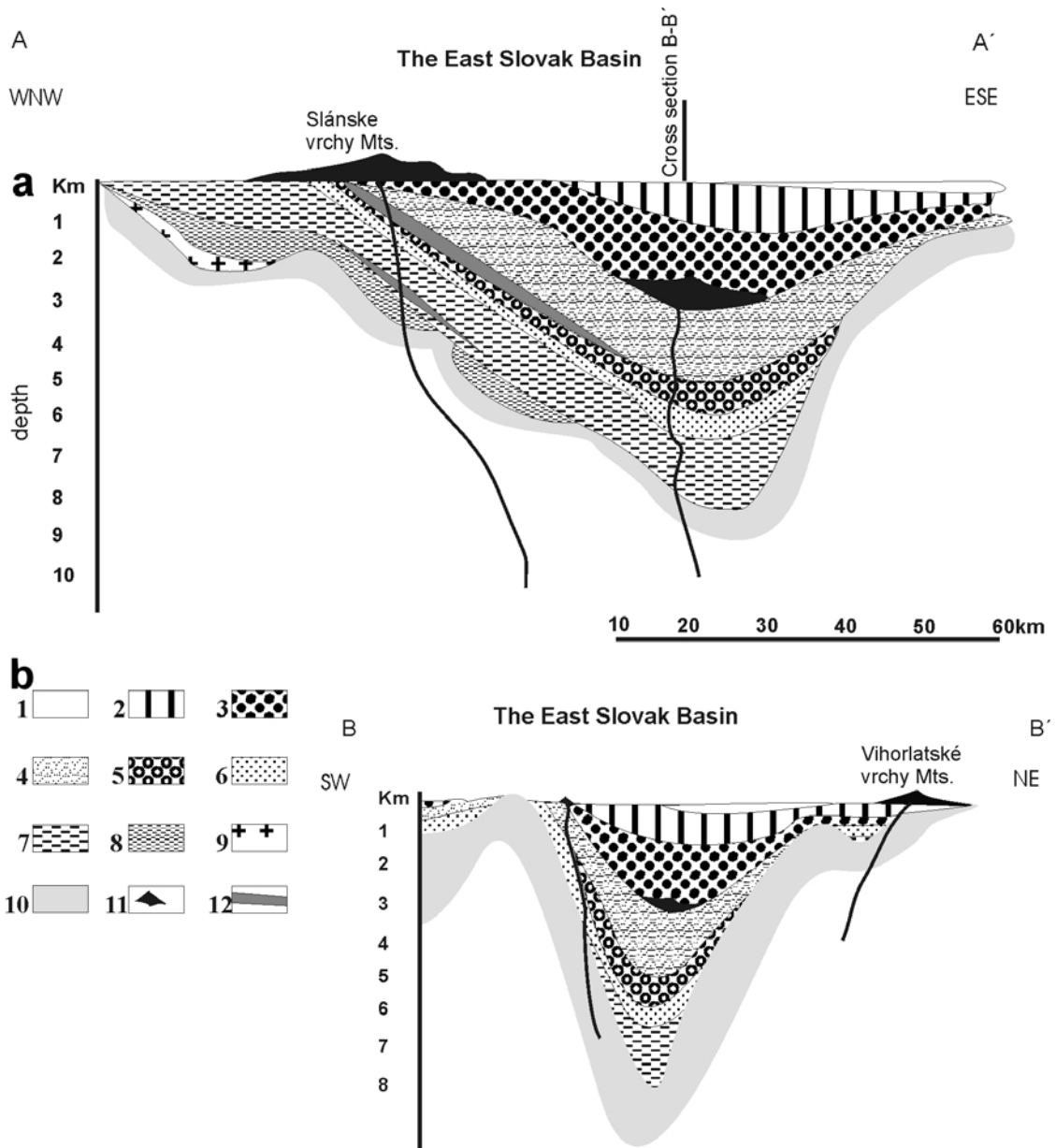
Figure 4. (a) AA′ Schematic longitudinal and (b) BB' transverse cross section of the Neogene sedimentary fill in the East Slovak Basin (after Rudinec, 1990). Legend: (1) Pliocene, (2) Pannonian to Pontian, (3) Sarmatian, (4) Upper Badenian, (5) Middle Badenian, (6) Lower Badenian, (7) Carpathian, (8) Eggenburgian, (9) Egerian, (10) pre-Neogene basement, (11) Neogene volcanics, (12) salt.

The PVP-10 separates the illite fundamental particles of the mixed-layer crystals. After the embedding of PVP-intercalated <2 μm fraction (Tessier, 1984; Elsass *et al.*, 1998) and polymerization of the resin, ultrathin sections (~70 nm thick) were cut using a Reichert Ultracut E microtome and a diamond knife. The HRTEM was performed using a JEOL JEM-2000 FX microscope operated at 160 kV with an objective aperture of 50 μm. Images taken at magnification 60,000 × in underfocus conditions were analyzed using a binocular microscope at a magnification between 10 and 40 × .

The illite crystal-thickness distributions (CTDs) were used to deduce the illitization mechanism in SBB. The measured CTDs were compared to calculated shapes of CTDs using the GALOPER computer program (Eberl *et al.*, 2001). The size of critical nucleus was set to 2 nm when the modeling results were compared to BWA-PVP data. The other input data were set by trial and error. The success of the simulation was evaluated by statistical tests (Kolmogorov-Smirnov and χ^2). The significance level $\alpha > 1$ was critical for accepting or rejecting the model.

Table 1. The borehole names, cores, depths, stratigraphy and XRD expandability (% S_{XRD}) of I-S in salt-bearing bentonites (SBB), salt-free bentonites (SFB) and shales of the East Slovak Basin used in this study.

	Borehole #	Borehole	Core #	Depth (m)	Stratigraphy	S_{XRD}
Salt-bearing bentonites	1	Bánovce 13	12	3313	Lower Badenian	5
	2	Bidovce 1	3/1	1565	Lower Badenian	70
	3	Hrušov 1	3A/1	955	Middle Badenian	92
	4	Pavlovce 1	7	2374	Middle Badenian	22
	5	Pozdišovce 7	29/1	2459	Lower Badenian	11
	6	Ptrukša 13	14	2100	Upper Badenian	13
	7	Ptrukša 47	9/7	2106	Middle Badenian	25
	8	Ptrukša 56	2/2	2065	Middle Badenian	10
	9	Senné 13	5A	2402	Middle Badenian	15
	10	Senné 21	4/1	2311	Middle Badenian	10
	11	Senné 45	1/5	2350	Middle Badenian	15
Salt-free bentonites*	12	Bánovce 4	1	602	Upper Sarmatian	100
	13	Blatná Polianka 1	1	746	Upper Sarmatian	95
	14	Čičarovce 1	12	1703	Lower Sarmatian	85
	14	Čičarovce 1	18	2296	Lower Sarmatian	51
	14	Čičarovce 1	20	2495	Lower Sarmatian	45
	15	Čičarovce 2	13	1808	Sarmatian	78
	15	Čičarovce 2	16	2119	Sarmatian	68
	16	Čičarovce 8	5a	2194	Lower Sarmatian	62
	16	Čičarovce 8	6	2431	Lower Sarmatian	60
	16	Čičarovce 8	11	2726	Lower Sarmatian	33
	17	Ďurkov 1	11	1060	Lower Sarmatian	87
	17	Ďurkov 1	11a	1062	Lower Sarmatian	88
	18	Ptrukša 10	10	1805	Sarmatian	60
	19	Ptrukša 20	5	1540	Sarmatian	90
	20	Ptrukša 22	-	2502	Upper Badenian	35
	21	Ptrukša 26	-	1361	Sarmatian	85
	22	Ptrukša 28	-	1306	Sarmatian	85
	23	Ptrukša 30	10	1815	Sarmatian	58
	24	Stretava 28	2	1350	Sarmatian	95
	25	Trhovište 1	37	3015	Lower Badenian/Upper Carpathian	18
	26	Zatín 1	1	1007	Upper Badenian	87
	26	Zatín 1	2	1302	Upper Badenian	85
	26	Zatín 1	15/1	2497	Upper Badenian	65
	26	Zatín 1	23	2897	Middle Badenian	18
	26	Zatín 1	27/2	3100	Lower Badenian	13
	26	Zatín 1	39	3602	Lower Badenian	12
	27	Žipov 1	1	31	Pannonian/Pliocene	95
	27	Žipov 1	1a	62	Pannonian/Pliocene	100
	27	Žipov 1	2	91	Pannonian/Pliocene	90
Shales*	6	Ptrukša 13	13	1998	Upper Badenian	20
	7	Ptrukša 47	9/8	2106	Middle Badenian	20
	9	Senné 13	6	2400	Middle Badenian	20
	10	Senné 21	5/1	2397	Middle Badenian	17

* % S data from Šucha *et al.* (1993). The borehole numbers correspond to those in Figure 3 indicating the positions of the studied boreholes. Expandability was measured using the methods described by Środoń (1981) and Dudek and Środoń (1996).

The K-Ar isotopic analyses were performed on different size fractions following a procedure close to that described by Bonhomme *et al.* (1975). The samples were pre-heated at 80ºC overnight to reduce atmospheric Ar adsorbed on the clay mineral surfaces during sample handling. The K contents were measured by flame spectrophotometry with the precision of ±1%. The Ar isotopic ratios were determined on an upgraded AEI 20 mass spectrometer. The $^{40}Ar/^{36}Ar$ atmospheric ratio in the extraction line before analysis was 287.2 which is consistent with an atmospheric $^{40}Ar/^{36}Ar$ ratio of 295.5 (Nier, 1950). The international GLO glauconite standard was used as a control. Its radiogenic ^{40}Ar content at $24.73\pm0.3 \times 10^{-6}$ cm^3/g STP was in good agreement with the reference value, which is $24.85\pm0.24 \times 10^{-6}$ cm^3/g STP (Odin and Bonhomme, 1982). The K-Ar ages were calculated using the usual decay constants (Steiger and Jäger, 1977). Analysis of

Table 2. The chemical composition (g kg^{-1}) of leachates of SBB and SFB samples.

	Borehole	Core #	Na	Mg	K	Cl$^-$	Σ(Na,Mg,K)
SFB	Čičarovce 8	5a	0.875	0.04475	0.177	0.53	1.09675
	Zatín 1	39	0.5645	0.03435	0.3485	0.5325	0.94735
	Čičarovce 1	12	1.325	0.01425	0.2655	0.8475	1.60475
	Ptrukša 20	5	3.02	0.00755	0.216	0.7625	3.24355
	Čičarovce 1	20	2.30	0.0009	0.1375	0.425	2.4375
	Trhovište 1	37	1.24	0.0009	0.218	1.385	1.455
SBB	Bánovce 13	12	2.05	0.0495	0.525	5.553	2.6245
	Hrušov 1	3A/1	7.40	0.0015	0.05	5.206	7.4515
	Ptrukša 47	9/7	4.50	0.0009	0.25	4.859	4.75
	Senné 45	1/2	4.05	0.0015	0.405	4.5115	4.4565
	Pavlovce 1	7	4.85	0.044	0.35	3.794	5.244
	Senné 13	5A	2.30	0.005	0.265	3.4705	2.57

all size fractions for each sample was not possible because the amounts of extracted material were limited.

The thermal maturity of organic matter dispersed in sediments (kerogen) was measured as random vitrinite reflectance, R_r, and as the T_{max} index of the Rock-Eval pyrolysis in shales adjacent to salt-bearing bentonites. The vitrinite reflectance was measured in oil on polished surfaces using a Leitz Wetzlar MPV2 microscope-photometer, with a $50 \times$ objective and Leitz standards of 1.26 and 5.42% reflectance (R_o) in non-polarized light at 546 nm. The measured thermal maturity indicators and the values for shales of several entire borehole profiles (Franců *et al.*, 1990) are used to distinguish between thermal and lithological or chemical factors influencing illitization.

The burial and thermal history was simulated using 1D PDI-PCTM forward modeling (PetroMod software). The process of model building is explained, for example, by Poelchau *et al.* (1997). The calculations included heat transfer during burial, compaction and thermal maturation of organic matter (EasyRo %) based on chemical kinetic equations following Sweeney and Burnham (1990). The model was calibrated by the measured random vitrinite reflectance (R_r %) and the present-day temperatures (Král *et al.* 1985). The simulated data on the diagenetic and catagenic alteration of the sediments were compared to the parameters measured in the boreholes, mutual agreement being a prerequisite for the validity of the burial and thermal evolutionary model.

RESULTS

Chemical composition of the leachates

The most significant difference in the chemical composition of the leachates from SBB and SFB is their chloride content (Table 2). Good separation of the SBB and SFB can be obtained when plotting the Cl content against the sum of cations (Figure 5). The Na and K contents are moderately higher in the SBB leachates relative to the SFB leachates. The Na content is about ten times higher than the K content. The Mg content varies between 0.005 and 0.0495 g kg^{-1} and that of SO_4 is always <0.5 g kg^{-1} except for one sample, where it reached 0.97 g kg^{-1}. There is no clear relationship between the chemical composition of the leachates and the degree of illitization in SBB. The Na, as the most abundant cation in the leachates, gives a poorly defined logarithmic curve with the expandability values (Figure 6). The least illitized sample (Hrušov 1 3A/1) with an expandability of 92% has the most concentrated leachate composition. The leachates of the moderately illitized SBB (~20% expandability) contain 4−5 g kg^{-1}
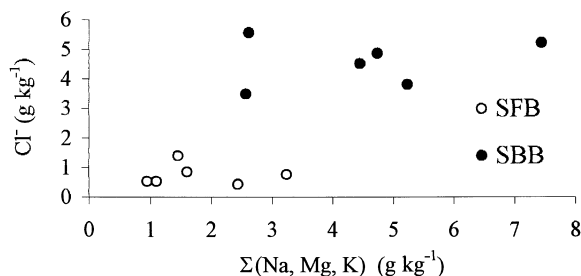

Figure 5. Cl contents related to the sum of cations determined in the leachates of the SFB (open circles) and SBB samples (filled circles).
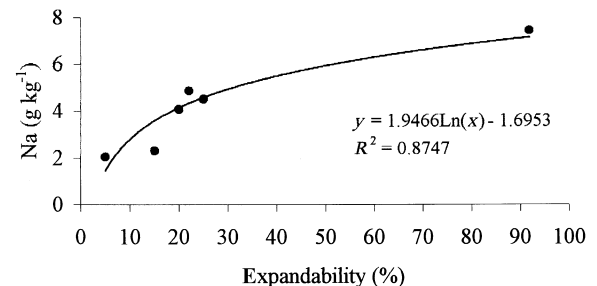

Figure 6. Na contents in leachates of the SBB samples related to the degree of illitization (expressed as % smectite content).
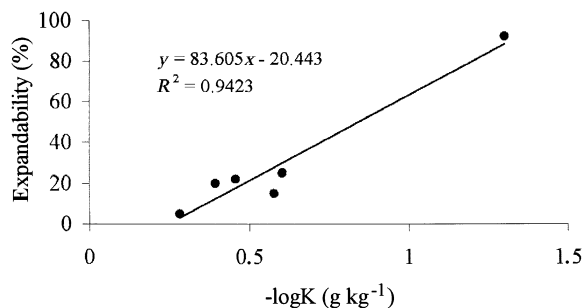
Figure 7. K contents (expressed as −logK) in leachates of the SBB samples related to the expandability values.

Na. The total concentration of cations is <3 g kg^{-1} in the most illitic samples (<20% expandability). A linear trend may be observed when plotting the K content, expressed as −logK against expandability (Figure 7). The most illitized sample has the highest K content in the leachate.

XRD of the clay fractions

The major mineral components (Figure 8) of the bulk SBB samples are quartz, albite, biotite, calcite and clay minerals ± zeolites (analcime, clinoptilolite). Gypsum was observed only in sample Bánovce 13/12. The XRD analyses of oriented specimens revealed the occurrence of clay minerals in the <2 μm fraction of all selected salt-bearing altered bentonites. Mixed-layer I-S domi-nated, in some cases even being the only clay mineral phase (Figure 9). The second major mineral phase was kaolinite. In some samples, both the <0.2 and <2 μm

fractions were analyzed, but no difference in expand-ability could be observed. Usually, the peaks were less noisy in the finer fraction. Measured expandability values of I-S were plotted as a function of depth (Figure 10), along with data for the SFB samples from a previous study (Šucha et al., 1993). Two samples (Hrušov 1 3A, S_{XRD} = 92%; Bidovce 1 3/1, S_{XRD} = 70%) fit the trend of the SFB well, but the remaining samples plot completely off the trend. In the depth interval between 1800 and 2500 m, corresponding to present-day burial temperatures of 90 to 130°C, the expandability values vary between 78 and 35%, with an R0 type I-S in the salt-free volcanoclastic rocks, and between 28 and 10% with an R1 or R3 I-S type, respectively, in the salt-bearing bentonites.

Particle-thickness distribution and GALOPER modeling

Illite particle-thickness distributions were measured using the HRTEM-PVP and BWA-PVP techniques in several SBB samples. In some cases (e.g. Senné 21 4/1 and Ptrukša 56 2/2 samples) the HRTEM-PVP and BWA-PVP distributions fit well, but in the others discrepancies arise between the two methods (Figure 11). Mostly HRTEM-PVP CTDs fit a theoretical lognormal curve, while BWA distributions approach an asymptotic shape of distribution (Kile et al., 2000). Mean particle thicknesses (T_{MEAN}) were calculated from all distribution patterns, along with two parameters: α (natural logarithm of the sizes) and β^2 (variance of the logarithms of the sizes), describing the shape of the particle distribution (Table 3). The HRTEM thickness was calculated including mono-
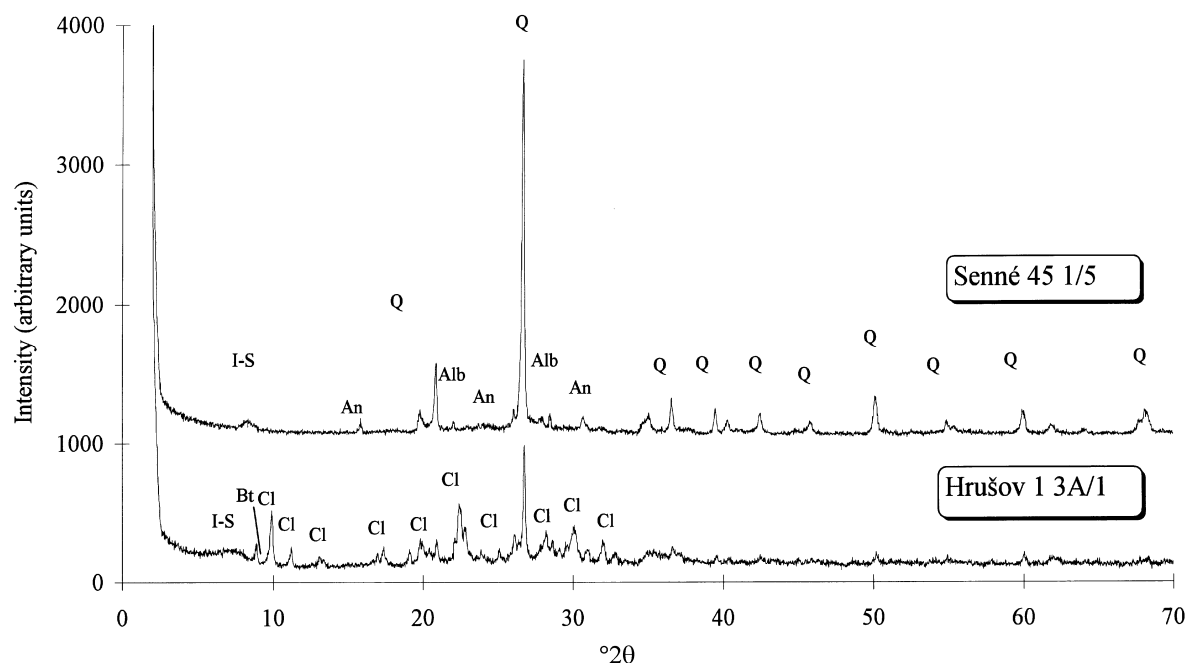

Figure 8. XRD patterns of random bulk SBB samples Senné 45 1/5 and Hrušov 1 3A/1. I-S − mixed-layer illite-smectite, An − analcime, Alb − albite, Q − quartz, Cl − clinoptilolite, Bt − biotite.
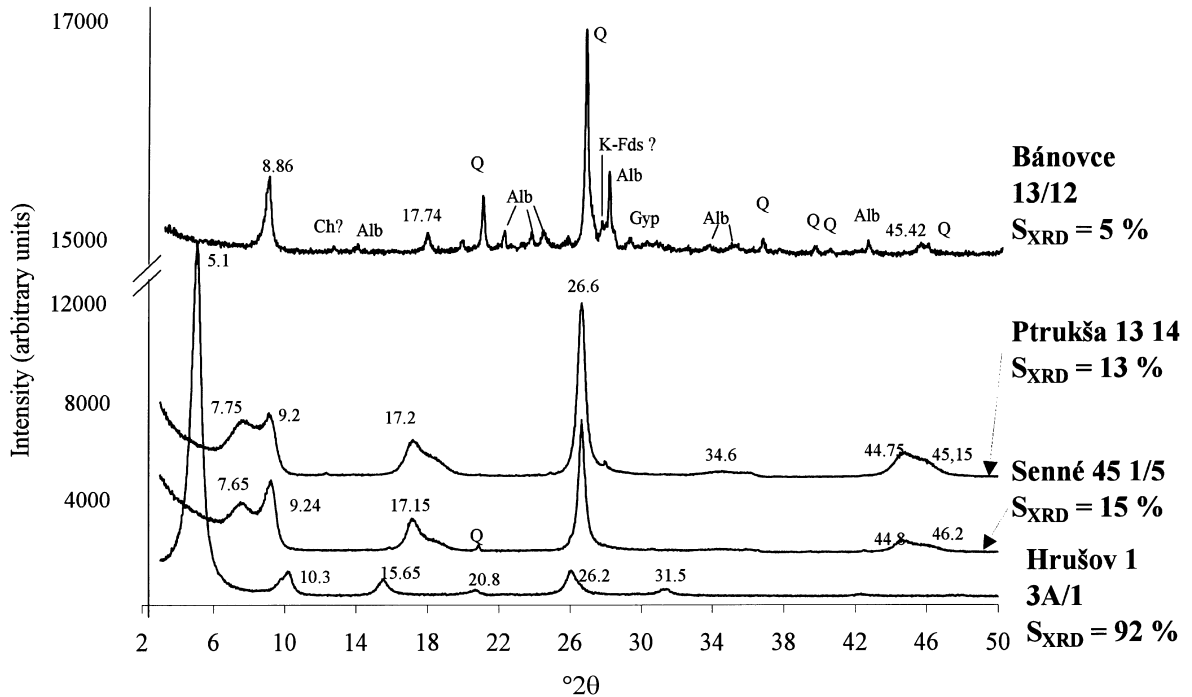
Figure 9. XRD patterns of ethylene-glycolated, oriented specimens of the SBB samples (<2 μm fraction). Ch − chlorite, K-Fds − K-feldspar, Gyp − gypsum, Q − quartz. Expandability measured by the X-ray peak-position method described by Dudek and Šrodoń (1996). I-S peaks marked with 2θ values.
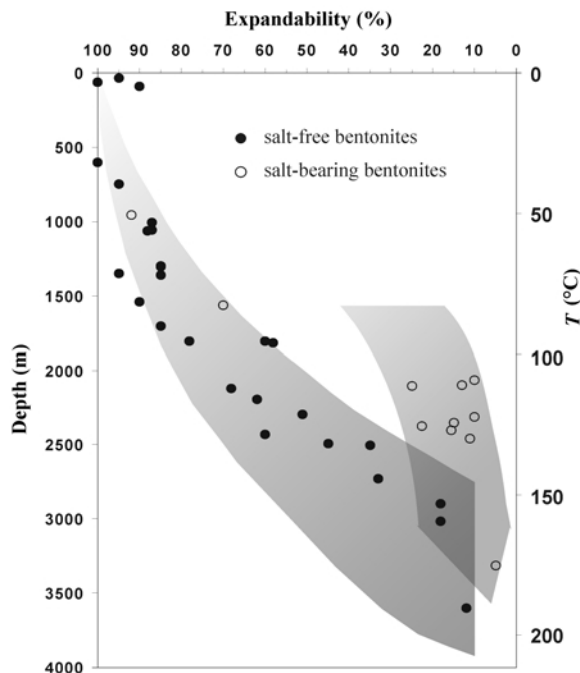

Figure 10. The illitization trends with depth/temperature in the East Slovak Basin for SFB (Šucha *et al.*, 1993) and SBB samples of the different boreholes. *T* (°C) are recent borehole temperatures measured by thermal logging (Král' *et al.*, 1985) or interpolated values calculated from heat-flow density.

layers (one 2:1 layer), which means that it cannot be compared directly to the BWA data, since XRD is unable to detect monolayers. Apart from sample Bánovce 13/12, BWA-PVP distributions give a systematically larger proportion of thick (>5 nm) and a smaller proportion of thin crystals in comparison with HRTEM-PVP distributions. Sample Bánovce 13/12 (5% S) illustrates the most extreme misfit between the two methods (Figure 11a). In this case, the BWA-PVP method detected a larger fraction of thin crystals and a smaller fraction of thicker ones compared to HRTEM-PVP.

The GALOPER modeling was applied to all K-Ar-dated samples except sample Bánovce 13/12. Simulated data were preferable to BWA-PVP data. The significant fit between BWA-PVP and GALOPER-simulated distribution in sample Senné 45 1/5 (Figure 12a) was acquired after running three crystallization cycles of simultaneous nucleation and surface-controlled growth followed by half a cycle of surface-controlled growth. This step was achieved by setting 500 crystals to nucleate per cycle and using the same number for a total number of crystals from 1001. The simulation was terminated by the input of 100 new 2 nm thick crystals into the system in order to meet the satisfactory result of statistical tests. In sample Senné 13 5A, four cycles of simultaneous nucleation and surface-controlled growth at a constant rate were applied to get the BWA-PVP distribution (Figure 12b). In sample Senné 21 4/1 the illite crystal growth was simulated by applying two cycles of constant-rate nucleation and growth in the first
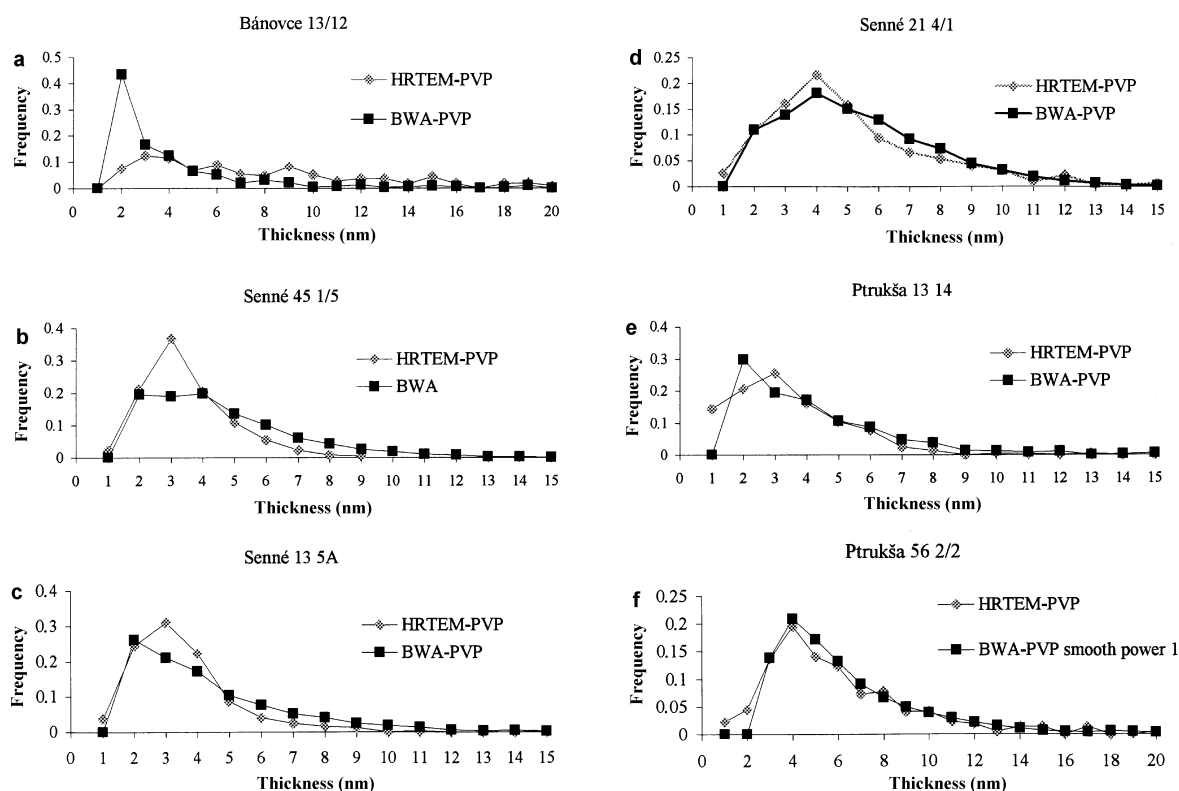
Figure 11. The particle thickness distributions, measured using the HRTEM-PVP and BWA-PVP techniques, of the (a) Bánovce 13/12, (b) Senné 45 1/5, (c) Senné 13 5A, (d) Senné 21 4/1, (e) Ptrukša 13 14 and (f) Ptrukša 56 2/2 samples.

step, two surface-controlled growth cycles in the next step and by adding 100 new 2 nm thick illite particles into the system at the end of the simulation (Figure 12c). The asymptotic pattern of the BWA-PVP data of sample Ptrukša 13 14 could be simulated by passing the crystals through four cycles of constant-rate nucleation and growth (Figure 12d).

K-Ar dating

The results of the K-Ar isotopic dating of five SBB are listed in Table 4. The K-Ar dates of the different size

fractions of sample Senné 45 1/5 increase with decreasing particle size fraction. Because all K-Ar dates of samples Senné 45 1/5, Senné 13 5A, Senné 21 4/1 and Ptrukša 13 14 are significantly lower than the stratigraphic age (15−15.5 Ma), they are considered to be illitization ages. The age of the coarsest fraction of sample Bánovce 13/12 is within the range of the depositional age. The presence of magmatic biotite was confirmed neither by XRD, nor by the energy dispersive microanalysis of 10 coarse particles. In spite of this, we consider the K-Ar ages reliable, the age of the coarsest

Table 3. α, β^2 and T_{mean} parameters calculated from crystal thickness distributions (CTDs) of the SBB samples determined using HRTEM-PVP and BWA-PVP methods. T_{mean} was calculated from the HRTEM-PVP data set including monolayers, but the α and β^2 parameters were calculated from these data excluding monolayers. n − number of measurements.

| | Borehole | Core# | HRTEM-PVP | | | | BWA-PVP | | |
			α	β^2	T_{mean}	n	α	β^2	T_{mean}
SBB									
	Bánovce 13	12	1.93	0.5	5.68	279	1.46	0.38	4.5
	Bidovce 1	3/1	0.83	0.06	1.28	494	−	−	−
	Hrušov 1	3A/1	0.76	0.03	1.09	781	−	−	−
	Ptrukša 13	14	1.24	0.17	2.88	285	1.3	0.27	4.2
	Ptrukša 47	9/7	1.07	0.18	2.83	148	1.03	0.21	3.07
	Ptrukša 56	2/2	1.70	0.27	5.28	220	1.49	0.32	5.32
	Senné 13	5A	1.20	0.15	3.16	242	1.34	0.28	4.4
	Senné 21	4/1	1.53	0.23	4.43	318	1.58	0.24	5.4
	Senné 45	1/5	1.20	0.12	3.21	128	1.33	0.26	4.3

fraction of sample Bánovce 13/12 being slightly contaminated by magmatic biotite or K-feldspar. The K-feldspar was identified in an oriented-specimen diffraction pattern of sample Bánovce 13/12 (Figure 9). The contamination effect disappears in two finer fractions, giving the same diagenetic age (12.5 Ma). As opposed to the Senné 45 1/5 sample, the K-Ar dates of the samples Senné 13 5A, Senné 21 4/1 and Ptrukša 13 14 decrease with decreasing particle size. The illitization ages ranged more widely in sample Senné 13 5A (10.3−2.2 Ma) than in samples Senné 21 4/1 (11.1−4.4 Ma) and Ptrukša 13 14 (10.6−7.2 Ma). The
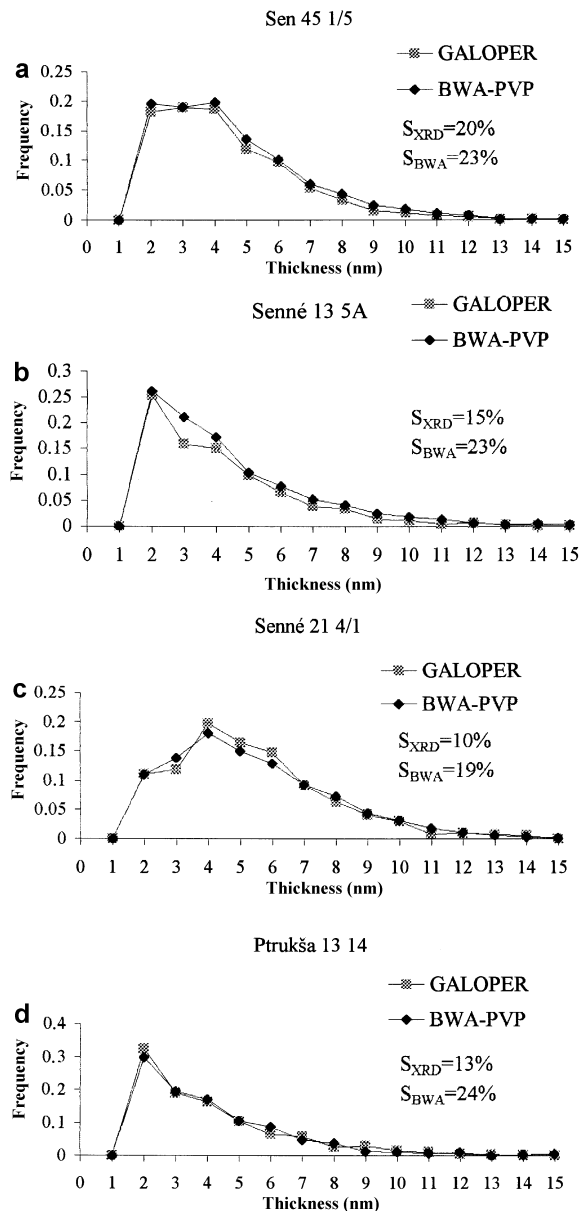
ages decrease with decreasing particle size and are inverse to increasing K_2O content.

Organic matter study

The increase in thermal maturity of organic matter with depth is rather steep in the ESB. At a depth of 4 km where the temperature is 200ºC, it is as high as the anthracite phase of coalification (Franců *et al.*, 1989). The general relationships of I-S expandability with depth and organic maturity in the East Slovak Basin are shown in Figure 13 for normal shales (Franců *et al.*, 1990) and SBB adjacent shales. The cross plot of expandability and vitrinite reflectance (Figure 13b) provides a closer correlation than % S with depth (Figure 10) as the effect of variations in geothermal gradient within the basin, small intrusions and erosion is eliminated. This is possible because both kerogen maturation and illitization are controlled mainly by complete thermal history. From Figures 13a and b it may be concluded that expand-
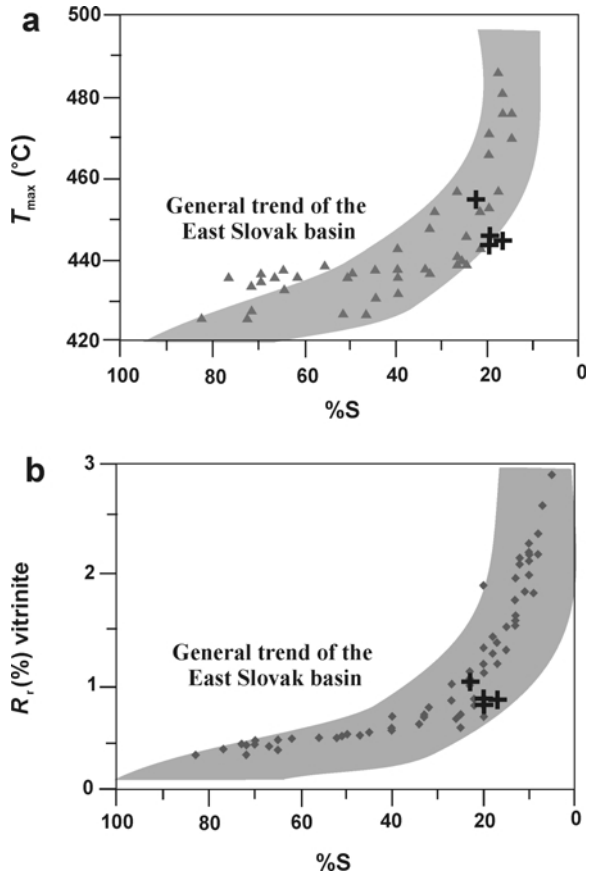

Figure 12. The BWA-PVP illite-thickness distributions compared to GALOPER-simulated distributions of the SBB samples.

Figure 13. Correlation of I-S expandability from XRD and organic maturity in the East Slovak Neogene Basin measured as (a) T_{max} (maximum pyrolytic temperature of the RockEval pyrolysis) and (b) R_o (vitrinite reflectance). Triangles and diamonds: T_{max} and R_o – data for shales of the different boreholes of the East Slovak Basin (Franců *et al.*, 1990). Crosses: T_{max} and R_o data for shales adjacent to SBB from Table 1.

Table 4. The K-Ar dates of different size fractions from five SBB samples.

	K_2O (%)	Ar* (%)	$^{40}Ar*$ (10^{-6} cm^3/g)	Age Ma±σ
Bánovce 13/12 (Lower Badenian ~16.5−15.5 Ma)				
2−0.2 mm	2.17	43.37	1.02	14.5 (0.9)
0.2−0.02 mm	5.92	32.93	2.39	12.5 (0.8)
<0.02 mm	6.32	44.83	2.56	12.5 (0.6)
Senné 45 1/5 (Middle Badenian ~15 Ma)				
2−0.2 mm	5.54	43.56	1.33	7.5 (0.4)
0.2−0.1 mm	6.95	28.23	1.74	7.8 (0.6)
0.1−0.02 mm	−	−	−	−
<0.02 mm	6.96	16.62	2.07	9.2 (1.1)
Senné 13 5A (Middle Badenian ~15 Ma)				
2−1 µm	4.33	11.3	1.45	10.3 (0.4)
1−0.2 µm	5.95	14.9	1.57	8.2 (0.2)
0.2−0.05 µm	6.93	14.5	1.14	5.1 (0.1)
0.05−0.02 µm	6.86	7.8	0.66	3.0 (0.1)
<0.02 µm	7.94	4.2	0.56	2.2 (0.1)
Senné 21 4/1 (Middle Badenian ~15 Ma)				
2−1 µm	2.87	16.8	1.03	11.1 (0.4)
1−0.2 µm	5.54	28.8	1.24	6.9 (0.1)
0.2−0.05 µm	7.98	16.2	1.03	4.0 (0.1)
0.05−0.02 µm	6.78	20.9	1.21	5.5 (0.1)
<0.02 µm	6.67	12	0.95	4.4 (0.1)
Ptrukša 13 14 (Upper Badenian ~14 Ma)				
2−1 µm	1.77	15.2	0.61	10.6 (0.4)
1−0.2 µm	4.17	29.2	1.09	8.1 (0.2)
0.2−0.05 µm	6.9	31.5	1.78	8.0 (0.1)
0.05−0.02 µm	6.92	22.9	1.71	7.6 (0.2)
<0.02 µm	6.94	16.8	1.61	7.2 (0.1)

The analytical error of the measurements was calculated using a formula derived by Cox and Dalrymple (1967).

ability, as well as the organic matter maturity of the shales adjacent to SBB, more or less fit the normal shale trend of the ESB determined for this lithology.

The correlation of expandability with the present borehole temperature is often insufficient for a thorough understanding of the effect of temperature on illitization, because geothermal gradient evolves with time, and uplift associated with erosion brings rocks to lower temperatures. Complete thermal history can be simulated using basin-modeling methods, and provides more precise information on diagenesis (Poelchau *et al.*, 1997). The model of burial and thermal history is shown for the Senne-45 borehole profile (Figure 14), with heat flow, depth below sediment surface, temperature and calibration by the measured organic maturity data (vitrinite reflectance). The input data of heat flow (Figure 14 bottom left) were modified stepwise until the modeled vitrinite reflectance trend fitted the measured data points. The burial history model of the borehole Senné 45 could be extrapolated for the majority of the studied boreholes, except for those located in the marginal parts of the basin. These areas are typical of the rapid tectonic subsidence during Carpathian and Badenian times followed by very slow or no tectonic

subsidence (see borehole Trhovište 1 in Clauer *et al.*, 1997). On the other hand, the burial model of borehole Senné 45 approaches the pattern reconstructed for the borehole Čičarovce 8 (Clauer *et al.*, 1997). It is characterized by slow tectonic subsidence throughout the geological history. The different tectonic history of these distinct areas is also reflected in the relative thicknesses of the sedimentary units (Figure 17). The resulting model shows that the studied salt-bearing volcanoclastic rock (bold line) experienced temperature in excess of 125ºC for the last 8 Ma. There is no evidence of erosion in the model. The slight temperature decrease during the last 2 Ma is due to compaction associated with an increase in overall heat conductivity of the lithological column and a general heat flow fading during the last 13 Ma in the ESB.

DISCUSSION

The studied samples generally occur as thin, altered, tuffitic beds intercalated in claystones or shales. According to Michalíček (1965, 1970), the Badenian groundwaters were affected by the hypersaline groundwaters of salt deposits as well as by groundwaters with
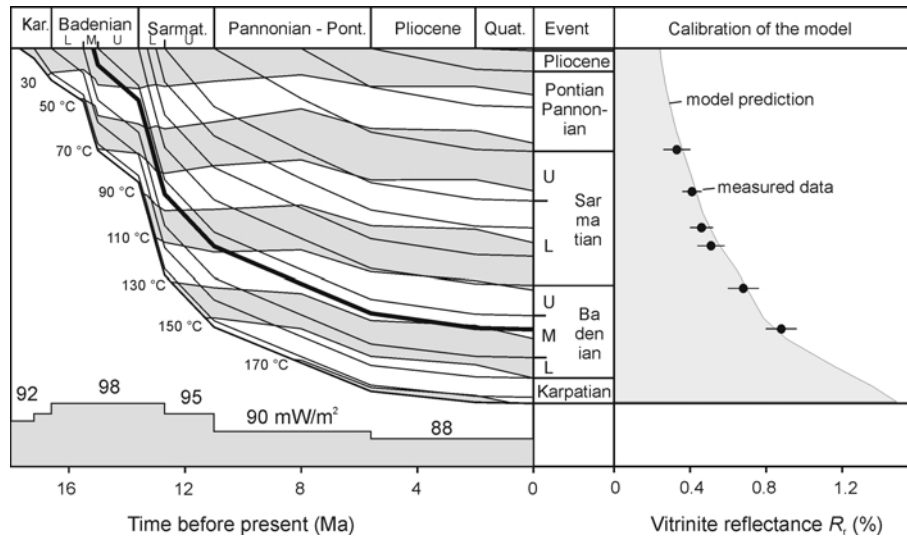
Figure 14. Burial and thermal history of the borehole profile Senne-45 calibrated by the vitrinite reflectance (right). The horizon with the salt-bearing bentonites is marked by the bold line. The heat-flow history is shown on the bottom left.

mineralization loads <30 g/L. The Badenian groundwaters of the ESB are clasified as brines or groundwaters of a salty origin. The brines seem to have originated by infiltration and subsequent leaching of salt deposits in Badenian units (Michalíček, 1970). This means that the SBB samples were probably in contact with a saline and/or hypersaline environment for an extended period of time. Brackish waters which were not mixed with brines are present in Upper Badenian and the Lower Sarmatian (Michalíček, 1970). Most of the studied SFB samples come from these stratigraphic units. Lack of evaporite minerals in SBB samples (except from Bánovce 13/12) imply that silica, enriched in the pore-waters from alteration of silicic glass, dominated reactions so that silicates precipitated rather than evaporites. The same effect was observed by Turner and Fishman (1991) in tuffs of a saline, alkaline Jurassic lake.

The salinity (Na and Cl contents) together with the degree of illitization are the principal differences between the SBB and SFB studied in the paper. The data show that the salinity was the principal factor enhancing illitization in the SBB along with the burial temperature. Other heat sources not induced by burial could be excluded because:

(1) the external heat source would have also affected the illitization and organic matter maturation degree in the shales hosting the salty bentonites, whereas comparison with existing data for claystones and shales of the ESB show no difference in either parameter (Figure 13a,b; Franců *et al.*, 1990; Šucha *et al.*, 1993).

(2) An external heat source would have led to the offset of the K-Ar data of all fractions, which is not the case. An external heat source (*e.g.* hydrothermal activity) causes the recrystallization which is accompanied by the loss of radiogenic Ar. The dating of such a sample shows equal ages for different fractions

indicating the time of the thermal event (Środoń *et al.*, 2002).

(3) No geological evidence of the occurrence of any volcanic body was found next to the SBB samples.

In the Gulf Coast region, highly smectitic I-S from deeply buried shales (~8 km) underlying the salt structures have been reported (D. McCarty, pers. comm.). There exist papers which state that salt structures within a sedimentary basin can modify its temperature distribution (*e.g.* Mello *et al.*, 1995). The salt structures channel heat from the bottom and sides towards the surface due to the higher thermal conductivity of salt relative to neighboring sediments. As a consequence, subsalt sediments, independent of their depth and lithology are colder than sediments with no salt. On the contrary, the positive thermal anomaly induces higher temperatures in the sediments located over the salt body. This was not the case for the SBB of the ESB. There is no direct presence of salt structures in the studied boreholes. Moreover, if lower than expected expandability of SBB resulted from elevated temperatures, it would also have affected the organic maturity of the studied shales (Figure 13a,b).

The salinity, as the sole factor leading to illitization immediately after deposition, as observed before in salt and/or alkaline lakes (Singer and Stoffers, 1980; Deconinck *et al.*, 1988; Hay *et al.*, 1991; Turner and Fishman, 1991) can be excluded as well. The influence of burial temperature is well documented by the time-temperature model of burial history combined with K-Ar data. A time-temperature model of progressive burial of the Senné 45 1/5 sample (Figure 14) shows that illitization was a temperature-controlled process, as for I-S from SFB samples (Clauer *et al.*, 1997). The occurrence of two 'salty' tuffs shallowly buried containing I-S with expandabilities fitting the trend of the SFB samples supports the

possibility that the impact of a salty environment becomes detectable after reaching a given (but so far unknown) temperature. Similarly, Środoń (1984) did not observe a catalytic effect of the saline-hypersaline environment on the illitization process in the shallow parts of Miocene in the Carpathian foredeep.

The exact mechanism of the salt-clay interaction during burial illitization is unclear and possibly very complex. Recent WD experiments (Honty *et al.*, 2003) show diverse effects of a saline environment on K fixation in smectites. The study emphasizes that lower NaCl concentrations significantly enhance K fixation, whereas high concentrations markedly slow down the process relative to a salt-free environment. A plot of Na concentrations in the leachates *vs.* expandability shows a similar effect (Figure 6). Accessibility of K in the system, expressed as −logK in Figure 7, probably played an important role during the smectite-to-illite alteration in the SBB.

The studies of Eberl *et al.* (1993) and Bauer and Velde (1999) showed that illitization is favored under high-pH conditions. The presence of analcime and clinoptilolite (Figure 8) suggests that the illitization in SBB occurred in an alkaline environment. Scanning electron microscopy images of the SBB sample Senné 45 1/5 indicate that the zeolites could have formed at any time of illitization (Figure 15). Figure 15a could be interpreted as the formation of analcime (by the alteration of volcanic glass) and subsequent crystallization of globular illite in free pore spaces. On the other hand, the idiomorphic crystals of analcime (Figure 15b) imply that in this case the zeolitization could have taken place after (some) illite crystallization (cycle). The SEM data cannot be used as evidence that

zeolitization progressed throughout the whole illitization process, but it is probable that the alkaline conditions prevailed at least at some point during illite formation. Although the experiments of Eberl *et al.* (1993) and Bauer and Velde (1999) were carried out at pH exceeding that in natural environments, the favorable effect of mild alkaline conditions together with slightly elevated temperature cannot be ignored.

The CSDs of the clay particles from SBB combined with K-Ar data were used to deduce the most likely illitization mechanism. The measured CSD shape can reveal information about crystal growth history because the shapes of CSDs are reaction-path dependent (Eberl *et al.*, 1998b). The α and β^2 data from I-S of the SBB samples obtained by BWA and HRTEM-PVP techniques were plotted on the diagram (Figure 16) along with the I-S data of diagenetically altered Carboniferous bentonites from the Upper Silesia Coal Basin, Miocene bentonites (SFB) from the East Slovak Basin (Środoń *et al.*, 2000) and hydrothermal bentonites (Eberl *et al.*, 1998a). The data set from SFB follows the trend which is characteristic for simultaneous nucleation and growth of the particles at the beginning and then dominated by surface-controlled growth (Eberl *et al.*, 1998b). The data from the same technique applied to the I-S of the SBB samples appear much more scattered. Some of them overlap the same trend (two highly expandable I-S from shallowly buried SBB − numbers 2 and 3 in Figure 16), but most of them show a significantly higher influence of simultaneous nucleation and growth. The scatter of data in Figure 16 does not allow for the assignment of a specific illitization growth mechanism for SBB clays on the basis of α *vs.* β^2 plot. A possible reason for the discrepancy between HRTEM-PVP and BWA-PVP data
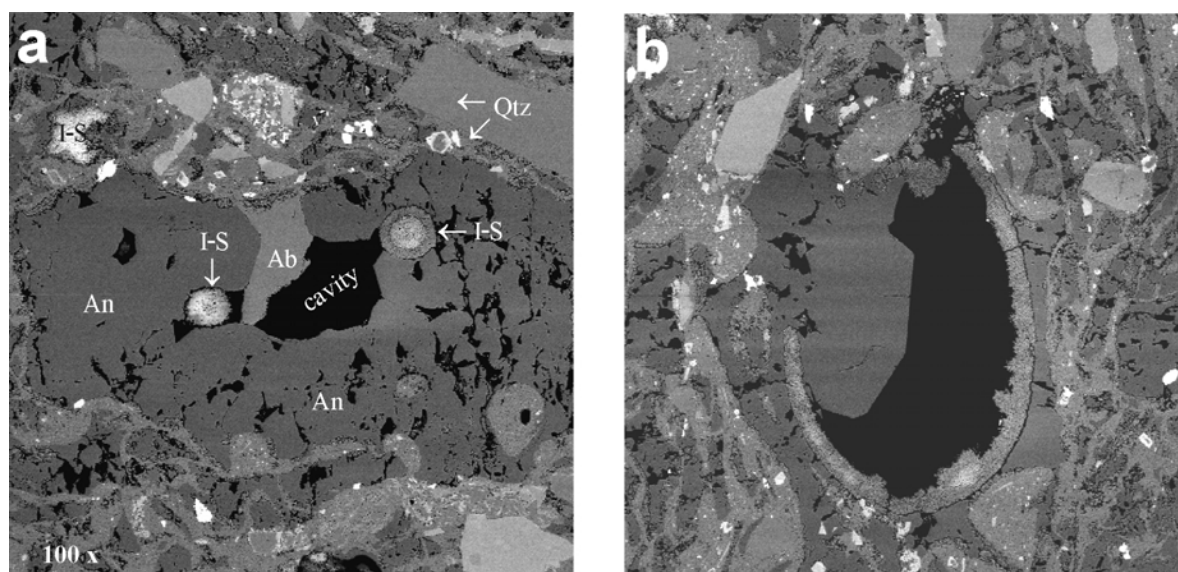

Figure 15. SEM images of the SBB sample Senné 45 1/5 (the whole-rock thin-section). (a) The anhedral analcime crystals in matrix and globular I-S filling the pore spaces. (b) The I-S crystals bordering the cavity rim. An − analcime.
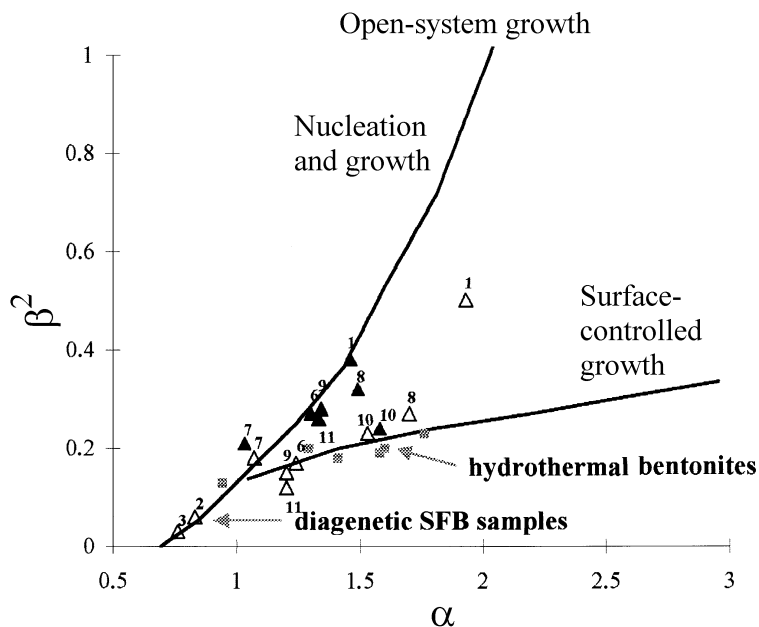
Figure 16. α *vs.* β^2 plot of SBB samples measured using the BWA-PVP (filled triangles) and HRTEM-PVP (open triangles) techniques. Filled squares represent the data for diagenetic bentonites from the Upper Silesia Coal Basin, the Miocene East Slovak Basin (Środoń *et al.*, 2000) and hydrothermal bentonites (Eberl *et al.*, 1998a). The samples are identified with the borehole numbers from Table 1. Theoretical curves of nucleation and growth and surface-controlled growth mechanism after Eberl *et al.* (1998b).

in shales was explained by Dudek *et al.* (2002). The BWA-PVP distributions, which are based on area-weighted frequencies, give a larger proportion of thick crystals than do HRTEM-PVP distributions, which are number weighted. This effect should not be pronounced in the particle size range typical for bentonites. In clays with T_{mean} <10 nm, area-weighted and number-weighted distribution parameters provide very close results (Środoń *et al.*, 2000). Our data indicate that the underestimation of the proportion of thick particles by HRTEM (due to insufficient counting statistics) when compared to the BWA technique (Figure 11) cannot be excluded even in the case of bentonitic samples. The same discrepancy between HRTEM and BWA particle thickness distributions of PVP-treated bentonites exists in data given by Dudek *et al.* (2002). Therefore, we rely more on BWA data, which are not dependent on the number of measurements, and use them for further interpretation.

The BWA-PVP particle-thickness distributions were simulated individually for selected SBB samples by GALOPER. The lognormal shape of the measured and simulated distributions of the sample Senné 45 1/5 (Figure 12a) is characteristic of a surface-controlled growth mechanism (Eberl *et al.*, 1998b). It is consistent with K-Ar data, when the finest crystals are the oldest (Table 4), representing the leftovers from the nucleation having taken place at the beginning of the process. Large particles are then younger, due to progressive, size-dependent overgrowth by younger material. The simulation of BWA-PVP measured distribution of Senné 21 4/1

sample (Figure 12c) confirmed the role of a surface-controlled growth mechanism after having experienced constant-rate nucleation and growth. A surface-controlled growth mechanism changes the asymptotic shape of the distribution to lognormal (Eberl *et al.*, 2001). The GALOPER simulation is in good agreement with the K-Ar data, which also reflects the impact of dual mechanism – decreasing ages in coarser fractions as a result of nucleation and growth and slight increase of ages in finer fractions as a consequence of surface-controlled growth. Finally, the GALOPER simulation of BWA distribution of sample Senné 13 5A and its asymptotic shape point to the illitization by constant rate nucleation and growth mechanism (Figure 12b). To the best of our knowledge, the simultaneous nucleation and growth mechanism is the only one to explain the observed K-Ar data of decreasing ages with decreasing particle size. The mechanism of simultaneous nucleation and growth accounts for the formation of new (and thus the finest) crystals at the end of the illitization reaction. The general decrease of K-Ar ages with decreasing size fraction confirms the ultimate importance of nucleation and growth in the illitization of sample Senné 13 5A (Table 4). The GALOPER modeling and K-Ar data of sample Ptrukša 13 14 show a similar growth mechanism (Figure 12d, Table 4). Provided that the SBB samples Senné 13 5A, Senné 21 4/1 and Senné 45 1/5 (15, 10 and 15% S_{XRD}, respectively) experienced very similar thermal histories, the different illite growth mechanisms in these samples could reflect the subtle changes in geochemistry of salt-rich solutions.
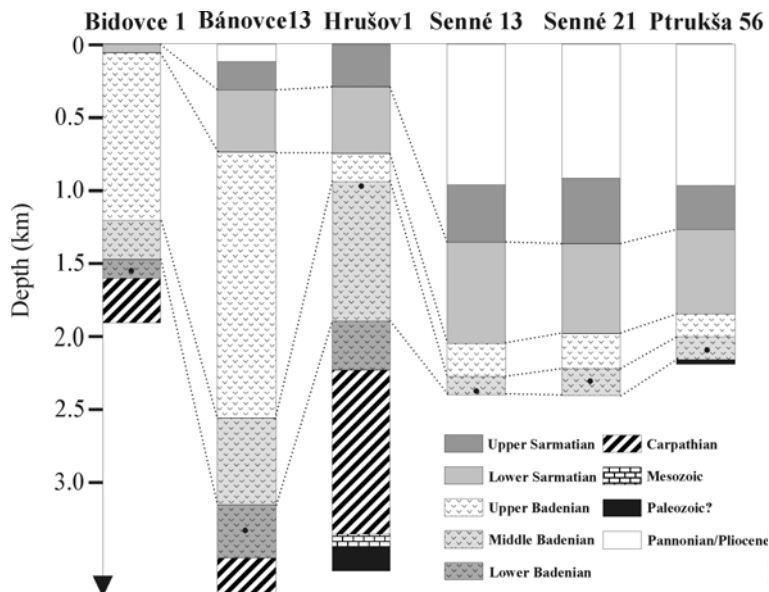
Figure 17. The stratigraphic correlation of the boreholes containing SBB samples.

The polymodal character of BWA-PVP and HRTEM-PVP distributions of the Bánovce 13/12 sample disabled the reasonable simulation of this sample by GALOPER. The striking difference between the HRTEM-PVP and BWA-PVP distributions, notably in the frequency of thick particles, could be attributed to the structural defects in coarse particles. These defects probably decreased the size of coherently diffracting domains. As a consequence, the frequency of bilayers increased dramatically in the BWA-PVP distribution compared to the HRTEM-PVP distribution. No variation between ages of two finer fractions of sample Bánovce 13/12 could be attributed to short-lived illitization. According to Środoń et al. (2002), equal ages for the various size fractions are characteristic of fast burial and/or of a hydrothermal event. The authors give as an example of fast burial, Miocene bentonite Trhovište 1/37. Borehole Bánovce 13 is close to borehole Trhovište 1 (Figure 3). For this reason we expect the burial history model of borehole Bánovce 13 to be similar to that determined in borehole Trhovište 1 (Clauer et al., 1997). Two finer fractions of sample Bánovce 13/12 giving the same diagenetic age thus indicate rapid subsidence of the region. Fast burial is also marked in the thickness of sedimentary units relative to the other studied boreholes of the SBB (Figure 17). The age of the coarsest fraction of sample Bánovce 13/12 (14.5 Ma) is probably contaminated by magmatic K-feldspar and, within the error limit, dates the time of sedimentation.

Eberl et al. (1993) and Bauer and Velde (1999) addressed the problem of using bentonites in combination with cement in the design of radioactive waste disposal sites. The authors attributed the possible loss of the desirable properties of bentonite to the alkaline effect of cement pore waters causing the formation of highly illitic I-S from smectite. It was documented that the saline environment promoted the illitization of smectite in SBB relative to SFB in the ESB. Therefore, the effect of saline environment should be also taken into account when salt domes are proposed as host rocks in combination with bentonites for nuclear waste storage.

CONCLUSIONS

The enhancing effect of a salty environment on the smectite to illite alteration was documented in salt-bearing bentonites of the East Slovak Basin. The chemistry of brine waters together with burial temperature were the most likely parameters controlling illitization in these salt-bearing bentonites. Investigation of CSD and K-Ar data were used to deduce the growth mechanism of illitization in SBB. Results show that the crystal growth mechanism probably varies according to the chemistry of the salt environment. It is evident that the simultaneous nucleation and growth played a more important role in the salt-bearing volcanoclastic samples than in the salt-free volcanoclastic samples. The study of illitization in saline environments shows that the smectite to illite transition has limited use in the reconstruction of thermal history of sedimentary basins and may have severe consequences for the utilization of bentonites as retaining barriers in the radioactive waste disposal sites if the salt effect cannot be excluded.

REFERENCES

Baráth, I., Kováč, M., Soták, J. and Lankreijer, A. (1997) Tertiary collision, metamorphism and basin forming processes in the Eastern Slovakia (central Western Carpathians). Pp. 65−78 in: *Geological Evolution of the Western Carpathians* (P. Grecula, D. Hovorka and M. Putiš, editors). Mineralia Slovaca − Monograph, Bratislava.

Bauer, A. and Velde, B. (1999) Smectite transformation in high molar KOH solutions. *Clay Minerals*, **34**, 259−273.

Bonhomme, M., Thuizat, R., Pinault, Y., Clauer, N., Wendling, R. and Winkler, R. (1975) Méthode de datation potassium-argon. Appareillage et technique. *Note technique de l'Institut de Géologie*, Université Strasbourg, **3**, 53 pp.

Clauer, N., Srodoň, J., Franců, J. and Šucha, V. (1997) K-Ar dating of illite fundamental particles separated from illite-smectite. *Clay Minerals*, **32**, 181−196.

Cox, A. and Dalrymple, G.B. (1967) Statistical analysis of geomagnetic reversal data and the precision of potassium-argon dating. *Journal of Geophysical Research*, **72**, 2603−2614.

Deconinck, J.F., Strasser, A. and Debrabant, P. (1988) Formation of illitic minerals at surface temperatures in Purbeckian sediments (Lower Berriasian, Swiss and French Jura). *Clay Minerals*, **23**, 91−103.

Drits, V.A., Eberl, D.D. and Środoń, J. (1998) XRD measurement of mean thickness, thickness distribution and strain for illite and illite/smectite crystallites by the Bertaut-Warren-Averbach technique. *Clays and Clay Minerals*, **46**, 461−475.

Dudek, T. and Środoń, J. (1996) Identification of illite/smectite by X-ray powder diffraction taking into account the lognormal distribution of crystal thickness. *Geologica Carpathica − Clays*, **5**, 21−32.

Dudek, T., Środoń, J., Eberl, D.D., Elsass, F. and Uhlík, P. (2002) Thickness distribution of illite crystals in shales. Part I: X-ray diffraction *vs.* high-resolution transmission electron microscopy measurements. *Clays and Clay Minerals*, **50**, 562−577.

Eberl, D.D. and Hower, J. (1976) Kinetics of illite formation. *Geological Society of America Bulletin*, **87**, 1326−1330.

Eberl, D.D., Środoń, J. and Northrop, H.R. (1986) Potassium fixation in smectite by wetting and drying. Pp. 296−326 in: *Geochemical Processes at Mineral Surfaces* (J.A. Davis and K.F. Hayes, editors). ACS Symposium Series, **323**, American Chemical Society.

Eberl, D.D., Velde, B. and McCormick, T. (1993) Synthesis of illite-smectite from smectite at earth surface temperatures and high pH. *Clay Minerals*, **28**, 49−60.

Eberl, D.D., Drits, V., Środoń, J. and Nüesch, R. (1996) *MudMaster: a program for calculating crystallite size distribution and strain from the shapes of X-ray diffraction peaks*. US Geological Survey, Open-File report 96−171.

Eberl, D.D., Nüesch, R., Šucha, V. and Tsipursky, S. (1998a) Measurement of fundamental illite particle thickness by X-ray diffraction using PVP-10 intercalation. *Clays and Clay Minerals*, **46**, 89−97.

Eberl, D.D., Drits, V.A. and Środoń, J. (1998b) Deducing growth mechanisms for minerals from the shapes of crystal size distributions. *American Journal of Science*, **298**, 499−533.

Eberl, D.D., Drits, V.A. and Środoń, J. (2001) *User's guide to GALOPER − a program for simulating the shapes of crystal size distributions−and associated programs*. US Geological Survey Open-File report OF00-505, 44 pp.

Elsass, F., Beaumont, A., Pernes, M., Jaunet, A.-M. and Tessier, D. (1998) Changes in layer organization of Na- and Ca-exchanged smectite materials during solvent exchanges for embedment in resin. *The Canadian Mineralogist*, **36**, 1475−1483.

Franců, J., Rudinec, R. and Šimánek, V. (1989) Hydrocarbon generation zone in the East Slovakian Neogene basin: model and geochemical evidence. *Geologický zborník.− Geologica Carpathica*, **40**, 355−384.

Franců, J., Müller, P., Šucha, V. and Zatkalíková, V. (1990) Organic matter and clay minerals as indicators of thermal history in the Transcarpathian depression (East Slovakian Neogene basin) and the Vienna basin. *Geologický zborník.− Geologica Carpathica*, **41**, 535−546.

Galamay, A.R. and Karoli, S. (1997) Geochemistry of the Badenian salts from the East Slovak basin (Slovakia). *Slovak Geological Magazine*, **3**, 187−192.

Hay, R.L., Guldman, S.G., Matthews, J.C., Lander, R.H., Duffin, M.E. and Kyser, T.K. (1991) Clay mineral diagenesis in core KM-3 of Searles Lake, California. *Clays and Clay Minerals*, **39**, 84−96.

Heller-Kallai, L. and Eberl, D.D. (1997) Potassium fixation by smectites in wetting-drying cycles with different anions. *Proceedings of the International Clay Conference, Ottawa*, pp. 561−567.

Honty, M., Šucha, V. and Magyar, J. (2002) Rock-facies dependent use of illite-smectite paleothermometry. *Mineralia Slovaca*, **34**, 29−34.

Honty, M., Šucha, V. and Puškelová, L. (2003) Potassium fixation in smectites by wetting and drying with NaCl solutions. *Geologica Carpathica*, **54**, 261−264.

Hower, J., Eslinger, E.V., Hower, M.E. and Perry, E.A. (1976) Mechanism of burial metamorphism of argillaceous sediment: 1. Mineralogical and chemical evidence. *Geological Society of America Bulletin*, **87**, 725−737.

Huang, W.-L., Longo, J.M. and Pevear, D.R. (1993) An experimentally derived kinetic model for smectite-to-illite conversion and its use as a geothermometer. *Clays and Clay Minerals*, **41**, 162−177.

Jackson, M.L. (1975) *Soil Chemical Analysis − Advanced Course*. Published by the author, Madison, Wisconsin, 386 pp.

Karoli, S. (1993) Evaporite facies in the Neogene East Slovakia Basin. *Abstracts of the 8th Meeting of the Association of European Geological Societies, Budapest*.

Karoli, S., Janočko, J., Kotulák, P. and Verdon, P. (1997) Sedimentology of Karpatian evaporites in the East-Slovakian Neogene basin (Slovakia). *Slovak Geological Magazine*, **3**, 201−211.

Kile, D.E., Eberl, D.D., Hoch, A.R. and Reddy, M.M. (2000) An assessment of calcite crystal growth mechanisms based on crystal size distributions. *Geochimica et Cosmochimica Acta*, **64**, 2937−2950.

Kováč, M., Kováč, P., Marko, F., Karoli, S. and Janočko, J. (1995) The East Slovakian Basin − a complex back arc basin. *Tectonophysics*, **252**, 453−466.

Král', M., Lizon, I. and Jančí, J. (1985) *Geothermal Research in Slovakia*. Geofond, Bratislava (in Slovak).

Lexa, J., Konečný, V., Kaličiak, M. and Hojstričová, V. (1993) Distribution of the Carpathian Pannonian region volcanites in space and time. Pp. 57−71 in: *Geodynamick model a hlbinná stavba Západných Karpát* (M. Rakús and J. Vozár, editors). Konferencie−Sympóziá−Semináre, GÚDŠ Bratislava (in Slovak).

Mello, U.T., Karner, G.D. and Anderson, R.N. (1995) Role of salt in restraining the maturation of subsalt source rocks. *Marine and Petroleum Geology*, **12**, 697−716.

Michalíček, M. (1965) Příspěvek k hydrogeochemii a hydro-

geologii hlubinnch vod Trebišovské nížiny. *Geologické práce, Zprávy*, **35**, 167−185 (in Czech).

Michalíček, M. (1970) K původu chloridosodných solanek v miocénu trebišovské nížiny. *Sborník geologických věd, řada HIG*, **7**, 107−159 (in Czech).

Mosser-Ruck, R., Cathelineau, M., Baronnet, A. and Trouiller, A. (1999) Hydrothermal reactivity of K-smectite at 300ºC and 100 bar: dissolution-crystallization process and non-expandable dehydrated smectite formation. *Clay Minerals*, **34**, 275−290.

Nadeau, P.H. and Reynolds, R.C. (1981) Burial and contact metamorphism in the Mancos shale. *Clays and Clay Minerals*, **29**, 249−259.

Nier, A.O. (1950) A redetermination of the relative abundances of the isotopes of carbon, nitrogen, oxygen, argon and potassium. *Physical Review*, **77**, 789−793.

Odin, G.S. and Bonhomme, M.G. (1982) Argon behaviour in clays and glauconies during preheating experiments. Pp. 333−343 in: *Numerical Dating in Stratigraphy* (G.S. Odin, editor). John Wiley, New York.

Poelchau, H.S., Baker, D.R., Hantschel, T., Horsfield, B. and Wygrala, B. (1997) Basin simulation and the design of the conceptual basin model. Pp. 5−70 in: *Petroleum and Basin Evolution* (D.H. Welte, B. Horsfield and D.R. Baker, editors). Springer, Berlin, Heidelberg, New York.

Pollastro, R.M. (1993) Considerations and applications of the illite/smectite geothermometer in hydrocarbon-bearing rocks of miocene to mississipian age. *Clays and Clay Minerals*, **41**, 119−133.

Rudinec, R. (1989) New view on the paleogeographic development of the Transcarpathian Depression during the Neogene. *Mineralia Slovaca*, **21**, 27−42.

Rudinec, R. (1990) Vertical distribution of Neogene sediments in the transcarpathian depression. *Mineralia Slovaca*, **22**, 5, 393−397.

Singer, A. and Stoffers, P. (1980) Clay mineral diagenesis in two east African lake sediments. *Clay Minerals*, **15**, 291−307.

Środoń, J. (1981) X-ray identification of randomly interstratified illite-smectite in mixtures with discrete illite. *Clay Minerals*, **16**, 297−304.

Środoń, J. (1984) Mixed-layer illite-smectite in low-temperature diagenesis: data from the Miocene of the Carpathian foredeep. *Clay Minerals*, **19**, 205−215.

Środoń, J. (1995) Reconstruction of maximum paleotemperatures at present erosional surface of the Upper Silesia Basin, based on the composition of illite/smectite in shales. *Studia Geologica Polonica*, **108**, 9−20.

Środoń, J. and Eberl, D.D. (1984) Illite. Pp. 495−544 in: *Micas*

(S.W. Bailey editor). Reviews in Mineralogy, **13**, Mineralogical Society of America, Washington, D.C.

Środoń, J., Eberl, D.D. and Drits, V.A. (2000) Evolution of fundamental-particle size during illitization of smectite and implications for reaction mechanism. *Clays and Clay Minerals*, **48**, 446−458.

Środoń, J., Clauer, N. and Eberl, D.D. (2002) Interpretation of K-Ar dates of illitic clays from sedimentary rocks aided by modeling. *American Mineralogist*, **87**, 1528−1535.

Steiger, R.H. and Jäger, E. (1977) Subcommission on geochronology: convention on the use of decay constants in geo- and cosmochronology. *Earth and Planetary Science Letters*, **36**, 359−362.

Sweeney, J.J. and Burnham, A.K. (1990) Evaluation of a simple model of vitrinite reflectance based on chemical kinetics. *American Association of Petroleum Geologists Bulletin*, **74**, 1559−1570.

Šucha, V., Kraus, I., Gerthofferová, H., Peteš, J. and Sereková, M. (1993) Smectite to illite conversion in bentonites and shales of the East Slovak Basin. *Clay Minerals*, **28**, 243−253.

Tessier, D. (1984) Étude experimental de l'organisation des materiaux argileux. Dr. Science thesis, Université Paris VII, INRA, 361 pp.

Turner, C.E. and Fishman, N.S. (1991) Jurassic lake T'oo'dichi': a large alkaline, saline lake, Morrison formation, eastern Colorado Plateau. *Geological Society of America Bulletin*, **103**, 538−558.

Uhlík, P., Šucha, V., Elsass, F. and Čaplovičová, M. (2000) High-resolution transmission electron microscopy of mixed-layer clays dispersed in PVP-10: a new technique to distinguish detrital and authigenic illitic material. *Clay Minerals*, **35**, 781−789.

Vass, D. and Čverčko, J. (1985) Neogene Lithostratigraphic Units in the East-Slovakian Lowland. *Geologické Práce, Správy*, **82**, 111−126 (in Slovak).

Vass, D., Kováč, M., Konečný, V. and Lexa, J. (1988) Molasse basins and volcanic activity in West Carpathian Neogene − its evolution and geodynamic character. *Geologica Carpathica*, **39**, 539−562.

Whitney, G. (1990) Role of water in the smectite-to-illite reaction. *Clays and Clay Minerals*, **38**, 343−350.

Whitney, G. and Northrop, H.R. (1988) Experimental investigation of the smectite to illite reaction: dual reaction mechanisms and oxygen-isotope systematics. *American Mineralogist*, **73**, 77−90.